

**Weak localization and crossover from Lifshitz transition in two dimensions**Kai-He Ding,<sup>1,2,\*</sup> Zhen-Gang Zhu,<sup>3,4,5,†</sup> Yong-Le Hu,<sup>6</sup> and Gang Su<sup>4,5,7,‡</sup><sup>1</sup>*Department of Physics and Electronic Science, Changsha University of Science and Technology, Changsha 410076, China*<sup>2</sup>*Hunan Provincial Key Laboratory of Flexible Electronic Materials Genome Engineering, Changsha University of Science and Technology, Changsha 410076, China*<sup>3</sup>*School of Electronic, Electrical and Communication Engineering, University of Chinese Academy of Sciences, Beijing 100049, China*<sup>4</sup>*Theoretical Condensed Matter Physics and Computational Materials Physics Laboratory, College of Physical Sciences, University of Chinese Academy of Sciences, Beijing 100049, China*<sup>5</sup>*CAS Center for Excellence in Topological Quantum Computation, University of Chinese Academy of Sciences, Beijing 100190, China*<sup>6</sup>*College of Automobile and Mechanical Engineering, Changsha University of Science and Technology, Changsha 410076, China*<sup>7</sup>*Kavli Institute of Theoretical Sciences, University of Chinese Academy of Sciences, Beijing 100049, China*

(Received 10 May 2021; revised 5 June 2021; accepted 4 October 2021; published 21 October 2021)

Dirac point plays a crucial role in regulating electronic properties of topological semimetals. In two dimensions, the manipulation of Dirac points can spur a transition from Dirac semimetal through semi-Dirac phase to a gapped phase. Across such a so-called Lifshitz transition, we find that the quantum interference corrections to the conductivity  $\delta\sigma_{xx}$  and  $\delta\sigma_{yy}$  are always negative, giving rise to a weak localization behavior. The ratio  $\delta\sigma_{xx}/\delta\sigma_{yy}$  undergoes a transition from linear to parabolic dependence on the merging parameter across the Lifshitz transition, which leads to a crossover of the temperature dependence of the inverse inelastic scattering time  $1/\tau_e$  from  $\sim T$  to  $\sim T \ln(T_0/T)$ . This fingerprint behavior can be readily tested experimentally through merging Dirac points in two-dimensional lattices. This work presents an alternative perspective to understand weak localization through Lifshitz transition.

DOI: [10.1103/PhysRevB.104.155135](https://doi.org/10.1103/PhysRevB.104.155135)**I. INTRODUCTION**

Weak localization (WL) is a physical effect caused by quantum interference of conduction electrons on self-intersecting diffusive trajectories in disordered systems, which exists in a variety of systems such as one- and three-dimensional metals, metal-oxide-semiconductor (MOS) inversion layers, and other semiconductors, etc. [1]. It has become an important area in condensed matter physics. Graphene, as a typical two-dimensional (2D) system, hosts many unusual properties [2–7], and should be a new platform for studying the WL. However, both theoretical and experimental works show that the WL is absent in graphene [8,9]. The reason is that the energy spectrum of graphene consists of two Dirac points at the corners of the Brillouin zone [10]. The quasiparticles basically move around a single valley, and acquire a Berry phase of  $\pi$  [6,11–13], which leads to a destructive interference in a backscattering process. Nonetheless, these disincentives can be reduced by modifying electronic band structure and the symmetry of internal disorder [8,14–19].

By altering the nearest-neighbor hopping of graphene lattice, two Dirac points approach each other [20,21], and can merge into a single one [22,23], forming the so-called

2D semi-Dirac system with energy spectrum being linear along one direction and parabolic along the other. Such an anisotropic energy spectrum gives rise to a number of special properties such as strongly anisotropic diffusion transport [24], the splitting of the Landau level spectrum in a magnetic field [20,23,25], Bloch-Zener oscillations [26], and transition of Hall conductivity plateaus from the half-integer to integer [27]. Recently, moving and merging Dirac points have been experimentally implemented in artificial lattice systems like the 2D honeycomb optical lattice [28], photonic graphene [29], and microwave-induced analog of a honeycomb lattice [30]. The semi-Dirac energy spectrum is also realized in many solid systems such as the organic conductor  $\alpha$ -(BEDT-TTF)<sub>2</sub>I<sub>3</sub> [31–33], TiO<sub>2</sub>/VO<sub>2</sub> nanostructures [34], Bi-Sb thin films [35], puckered honeycomb arsenic systems [36], and black phosphorus [37,38], etc.

We identify that the merging Dirac points and reopening a gap is a kind of Lifshitz transition in which the topology of Fermi surfaces is altered. Conventionally, the Lifshitz transition is usually studied via energy dispersion and density of states due to its particular shape of Fermi surfaces. Here we show a deep connection between Lifshitz transition and weak localization. This may bring us a new direction to explore the particular effect of nontrivial Fermi surface topology on dynamical properties. We study the quantum interference corrections to conductivities  $\sigma_{\mu\mu}$  ( $\mu = x, y$ ) across the Lifshitz transition with the topology of spin rotation along the backscattering paths. The net spin rotation along the backscattering paths is zero, contributing a zero Berry phase across

\*dingkh@csust.edu.cn

†zgzhu@ucas.ac.cn

‡gsu@ucas.ac.cn

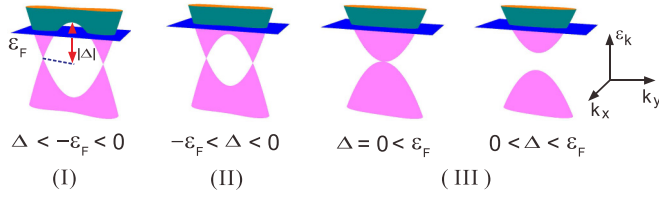


FIG. 1. Diagrams of energy spectrum for the Hamiltonian (1), where the absolute value  $|\Delta|$  denotes the saddle point energy. The Fermi surface (blue) intersects with the conduction band ( $\varepsilon_F > 0$ ). Filled eigenstates are represented by magenta regions.

the Lifshitz transition, such that  $\delta\sigma_{xx}$  and  $\delta\sigma_{yy}$  are always negative in the full merging parameter ( $\Delta$ ) region, marking a WL behavior. Meanwhile, the ratio  $\delta\sigma_{xx}/\delta\sigma_{yy}$  displays a constant independent of  $\Delta$  just around the merging point; while a linear dependence on  $\Delta$  for the two-Dirac-point case. This marks a characteristic feature for the Lifshitz transition manifesting in the WL. We further show that the Lifshitz transition induces a crossover of the temperature dependence of the inelastic scattering time  $\tau_\varepsilon$  from  $1/\tau_\varepsilon \sim T$  to  $1/\tau_\varepsilon \sim T \ln(T_0/T)$ .

## II. Theoretical model

An effective Hamiltonian describing the merging transition of Dirac points in two dimensions can be expressed as [20]

$$H = \left( \Delta + \frac{k_x^2}{2m} \right) \sigma_x + v_y k_y \sigma_y, \quad (1)$$

where  $m$  is the  $x$  direction band mass,  $v_y = 3$  at/2( $t = 2.3$  eV,  $a = 1.42$  Å) is the  $y$  direction Fermi velocity,  $\sigma_i$  ( $i = x, y$ ) are the Pauli matrices, and  $k_i$  is the wave vector. The eigenstates of the Hamiltonian (1) are given by  $|u_{\mathbf{k}}^+\rangle = \frac{\sqrt{2}}{2}(1, e^{i\phi_{\mathbf{k}}})^T e^{i\mathbf{k}\cdot\mathbf{r}}$  and  $|u_{\mathbf{k}}^-\rangle = \frac{\sqrt{2}}{2}(1, -e^{i\phi_{\mathbf{k}}})^T e^{i\mathbf{k}\cdot\mathbf{r}}$  with  $\tan \phi_{\mathbf{k}} = v_y k_y / (k_x^2/2m + \Delta)$ . The corresponding energy spectrum is  $\varepsilon_{\mathbf{k}}^\pm = \pm[(\Delta + \frac{k_x^2}{2m})^2 + (v_y k_y)^2]^{1/2}$ . The parameter  $\Delta$  presents the merging scenario of two Dirac points, as shown in Fig. 1. Two Dirac points remain apart from each other for  $\Delta < 0$ , and merge at  $\Delta = 0$ . A gap between the conduction and valence bands opens for  $\Delta > 0$ . Equation (1) is originally formulated in the context of graphene [20]. Various analogous systems [28,30,39] have paved the way to its physical realization, including new aspects that were addressed [40]. In this work, we focus on the quantum interference effect on transport from disorder scattering and screened Coulomb interaction, which is untouched so far.

We consider randomly distributed  $\delta$ -function  $V(\mathbf{r}) = \sum_i V_i \delta(\mathbf{r} - \mathbf{R}_i)$  to model the scattering by the impurities, where  $\mathbf{R}_i$  are the positions of the impurities, and  $V_i$  are the strength distributions of impurity potentials, satisfying  $\langle V_i \rangle_{\text{dis}} = 0$  and  $\langle V_i^2 \rangle_{\text{dis}} = V_0^2$ , where  $\langle \dots \rangle_{\text{dis}}$  means the average over the impurity configurations. All the calculations are performed in the thermodynamic limit, i.e., the system is taken as infinity. The Fermi level is introduced as an external parameter, revealing the variation of the impurity scattering, and can actually be changed by the gate voltage [18,41–43]. In the present work, we suppose the Fermi energy  $\varepsilon_F$  to be positive, i.e.,  $\varepsilon_F$  always crosses the conduction band. In the weak disorder limit, the energy width of Bloch state is

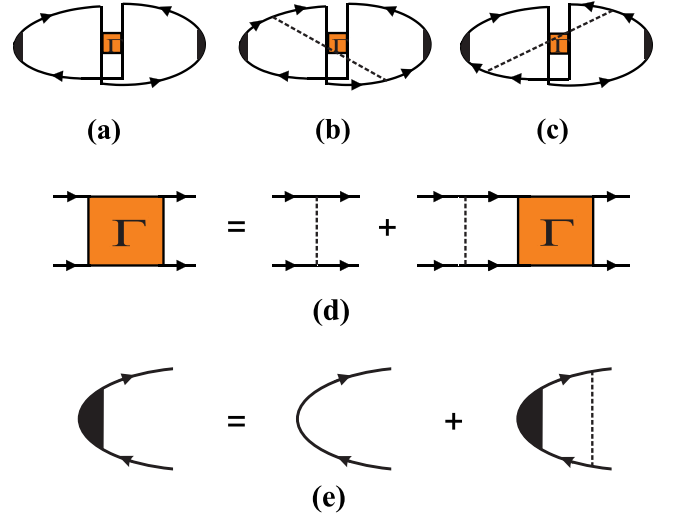


FIG. 2. Diagrams for the quantum interference correction to the conductivity, consisting of the bare Hikami box [44,45] (a) and the dressed Hikami boxes [16,41] (b) and (c). The Bethe-Salpeter equation for Cooperon is shown in (d). The arrowed lines represent the impurity-averaged Green's functions, and the dashed lines represent the impurity scattering. The dark regions on the two sides of each box stand for the vertex correction to velocity shown in (e).

small, therefore, we can neglect the interband scattering at zero temperature, and calculate all physical quantities in the conduction band.

## III. CONDUCTIVITY CORRECTIONS FORMULA

In order to get the quantum interference correction to the conductivity, we sum the maximally crossed diagrams including the bare Hikami box [44–46] and the dressed Hikami box [16,41], as shown in Figs. 2(a)–2(c). The calculation for the Hikami box is associated with two-particle correlation function called Cooperon, which satisfies the Bethe-Salpeter equation represented graphically in Fig. 2(d):

$$\Gamma_{\mathbf{k}\mathbf{k}'}(\mathbf{q}) = \Gamma_{\mathbf{k}\mathbf{k}'}^0 + \frac{1}{S} \sum_{\mathbf{k}_1} \Gamma_{\mathbf{k}\mathbf{k}_1}^0 G_{\mathbf{k}_1}^R G_{\mathbf{q}-\mathbf{k}_1}^A \Gamma_{\mathbf{k}_1\mathbf{k}'}(\mathbf{q}), \quad (2)$$

where  $\mathbf{q} = \mathbf{k} + \mathbf{k}'$ ,  $S$  is the area,  $G_{\mathbf{k}}^{R(A)}$  is the retarded (advanced) Green's function, and the bare Cooperon

$$\Gamma_{\mathbf{k}\mathbf{k}'}^0 = \frac{\hbar}{2\pi g_0 \tau_0} [1 + \cos(\phi_{\mathbf{k}} - \phi_{\mathbf{k}'})], \quad (3)$$

where  $g_0$  is the density of states, and the angular dependence term generated from the anisotropy in the energy spectrum. In Eq. (3), the elastic scattering time  $\tau_0^{-1} = \frac{\pi}{\hbar} n_i V_0^2 g_0$ , where  $n_i$  is the impurity concentration. Throughout the paper, we choose the parameters  $n_i = 10^{-3}$  Å<sup>-2</sup>, and  $V_0 = 6 \times 10^{-15}$  eV · cm<sup>2</sup>, such that the perturbative condition can be satisfied [6,47]. The crossed diagrams describe the interference of the time-reversed paths, and diverge in the limit of  $\mathbf{q} = 0$ . The Cooperon is therefore dominated by the contribution from values  $\mathbf{q}$  near zero. To acquire this contribution, we expand the advanced Green's function  $G_{\mathbf{q}-\mathbf{k}_1}^A$  up to the second order

of  $\mathbf{q}$ , and then by the iteration, we find

$$\Gamma_{\mathbf{kk}'}(\mathbf{q}) = \frac{\hbar^3 I_0}{2\pi g_0 \tau_0^3} \frac{1}{(2\varepsilon_F/m)D_x q_x^2 + v_y^2 D_y q_y^2}, \quad (4)$$

where

$$\begin{aligned} D_x &= \mathcal{K}_8 + 2\gamma\mathcal{K}_9 - \frac{\gamma\mathcal{K}_1(\mathcal{K}_8 - \mathcal{K}_{10})}{I_0 - \mathcal{J}_1 + \mathcal{K}_2}, \\ D_y &= \mathcal{K}_5 + 2\gamma\mathcal{K}_6 + \frac{\mathcal{K}_3^2}{I_0 - \mathcal{J}_1 + \mathcal{K}_2} - \frac{\gamma(\mathcal{K}_1\mathcal{K}_7 + 2\mathcal{K}_3\mathcal{K}_4)}{I_0 - \mathcal{J}_1 + \mathcal{K}_2}, \end{aligned} \quad (5)$$

where  $\gamma$ ,  $I_0$ ,  $\mathcal{J}_1$  and  $\mathcal{K}_i$ , ( $i = 1, 2, \dots, 8$ ) are expressed with the elliptic integrals (see Appendix D).

Using Eq. (4) and collecting all the contributions of Figs. 2(a)–2(c), we obtain the WL corrections to the quantum conductivities in  $x, y$  directions

$$\begin{aligned} \delta\sigma_{xx} &= -\frac{e^2}{\pi h} \sqrt{\frac{2\varepsilon_F}{mv_y^2}} \frac{\mathcal{K}_8}{\bar{D}} \ln\left(\frac{\tau_\varepsilon}{\tau_0}\right), \\ \delta\sigma_{yy} &= -\frac{e^2}{\pi h} \sqrt{\frac{mv_y^2}{2\varepsilon_F}} \frac{\alpha_0^2}{\bar{D}} \left(\mathcal{K}_5 - \frac{\mathcal{K}_3^2}{I_0}\right) \ln\left(\frac{\tau_\varepsilon}{\tau_0}\right), \end{aligned} \quad (6)$$

where  $\tau_\varepsilon$  is the inelastic scattering time,  $\bar{D} = \sqrt{D_x D_y}$ , and  $\alpha_0 = I_0/(I_0 - \mathcal{J}_1 + \mathcal{K}_2)$  comes from the correction of the velocity  $v_y$ , which is obtained from the ladder diagram in Fig. 2(e). Since the  $x$  component of the velocity is an odd function of  $k_x$ , there is no renormalization factor.

#### IV. INELASTIC SCATTERING TIME

We introduce the inelastic scattering time  $\tau_\varepsilon$  in Eq. (6), which is associated with the Coulomb interaction between electrons. In the presence of disorder, the Coulomb interaction is screened, and within the random phase approximation, has the form of

$$V(\mathbf{q}, \omega_m) = \frac{V_0(\mathbf{q})}{1 + V_0(\mathbf{q})\Pi(\mathbf{q}, \omega_m)}, \quad (7)$$

where  $\omega_m$  is the Matsubara frequency  $2\pi mT$  ( $m$  is an integer and  $T$  means temperature), the bare Coulomb interaction  $V_0(\mathbf{q}) = e^2/2\varepsilon q$  with  $\varepsilon$  the dielectric constant, and in the limit of  $\omega_m \rightarrow 0$  and  $q \rightarrow 0$ , the density-density response function  $\Pi(\mathbf{q}, \omega_m)$  is expressed as

$$\Pi(\mathbf{q}, \omega_m) = \frac{g_0[\beta|\omega_m| + (2\tau_0\varepsilon_F/m)D_x q_x^2 + \tau_0 v_y^2 D_y q_y^2]}{I_0|\omega_m| + (2\tau_0\varepsilon_F/m)D_x q_x^2 + \tau_0 v_y^2 D_y q_y^2} \quad (8)$$

with  $\beta = I_0 - \frac{\mathcal{J}_1^2}{I_0}$ .

Then, in terms of the diagrammatic technique [48], we obtain  $\tau_\varepsilon$  (for details refer to Appendix F)

$$\begin{aligned} \frac{1}{\tau_\varepsilon} &= -\frac{\mathcal{J}_1^2 T}{8\pi^3 g_0 V_+} \Im \int_0^{2\pi} d\varphi \frac{1}{1 + \nu \cos \varphi} \\ &\times \int_0^\infty dy \sum_{s=\pm} \left[ \frac{1}{I_0 y + s(\alpha y^{1/2} + \beta)(\frac{\tau_0}{\tau_\varepsilon} + y)} \right. \\ &\times \left. \log \frac{I_0 T \tau_0 + i(\frac{\tau_0}{\tau_\varepsilon} + y)}{-s(\alpha y^{1/2} + \beta)T \tau_0 + iy} \right], \end{aligned} \quad (9)$$

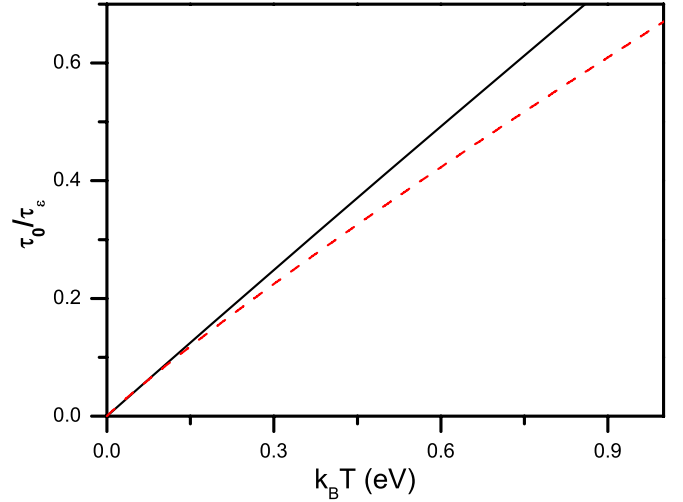


FIG. 3. The inverse inelastic scattering time as a function of temperature at  $\varepsilon_F = 2.0$  eV,  $m = 0.5$  eV $^{-1}$  Å $^{-2}$ , and  $v_y = 3.75 \times 10^5$  m/s. The parameter  $\Delta$  is taken as  $\Delta = -1.0$  eV and  $\Delta = -80.0$  eV for the solid (black) and dashed (red) lines, respectively.

where  $V_+ = \frac{1}{2}\tau_0 v_y^2 [(2\varepsilon_F/mv_y^2)D_x + D_y]$ , and  $\alpha = \frac{I_0}{\sqrt{\mathcal{A}(1+\nu \cos \varphi)}}$  with  $\mathcal{A} = (\frac{e^2 g_0}{2\varepsilon})^2 V_+ \tau_0$  and  $\nu = \frac{D_x - (mv_y^2/2\varepsilon_F)D_y}{D_x + (mv_y^2/2\varepsilon_F)D_y}$ .

From Eq. (9), the inelastic scattering time  $\tau_\varepsilon$  needs to be determined self-consistently. The numerical results show that  $1/\tau_\varepsilon$  has a linear or a nonlinear temperature dependence at  $|\Delta| < \varepsilon_F$  or  $\Delta < -\varepsilon_F$  (see Fig. 3). This characteristic behavior is further uncovered by the equations up to leading order in  $T$  for the following two cases:

(i) For  $|\Delta| < \varepsilon_F$ , i.e., the cases (II) and (III) in Fig. 1, substituting Eq. (8) into Eq. (7), and keeping the leading terms on small  $\omega_m$  and  $q$ , we get

$$V(\mathbf{q}, \omega_m) = \frac{I_0|\omega_m| + (2\tau_0\varepsilon_F/m)D_x q_x^2 + \tau_0 v_y^2 D_y q_y^2}{g_0\beta|\omega_m| + (2\tau_0\varepsilon_F/m)D_x q_x^2 + \tau_0 v_y^2 D_y q_y^2}, \quad (10)$$

which makes Eq. (9) become

$$\begin{aligned} \frac{\tau_0}{\tau_\varepsilon} &= \frac{\chi}{\varepsilon_F} \Re \int_0^T dz \frac{z}{\sinh z/T} \left[ \frac{-iI_0 z + \frac{1}{\tau_\varepsilon}}{\beta^2 z^2 + (-iI_0 z + \frac{1}{\tau_\varepsilon})^2} \right. \\ &\times \ln \left( \frac{-iI_0 z + \frac{1}{\tau_\varepsilon}}{\beta z} \right) \\ &\left. + \frac{\pi \beta z/2}{\beta^2 z^2 + (-iI_0 z + \frac{1}{\tau_\varepsilon})^2} \right], \end{aligned} \quad (11)$$

where  $\chi = \frac{\mathcal{J}_1^2}{I_0 \bar{D}}$ . We further estimate Eq. (11) for  $\tau_\varepsilon T \gg 1$ :

$$\frac{\tau_0}{\tau_\varepsilon} = \frac{T}{2\varepsilon_F} [\Lambda_1 \ln(\Lambda_2 T \tau_\varepsilon) + \Lambda_0], \quad (12)$$

where  $\Lambda_1 = \frac{\pi \mathcal{J}_1^2}{(2I_0^2 - \mathcal{J}_1^2)\bar{D}}$ ,  $\Lambda_2 = (2I_0^2 - \mathcal{J}_1^2)/I_0$ , and  $\Lambda_0 = \frac{\pi I_0^2}{(2I_0^2 - \mathcal{J}_1^2)\bar{D}} \ln(\frac{I_0^2}{I_0^2 - \mathcal{J}_1^2})$ . To the leading order in  $T$ , Eq. (12) is

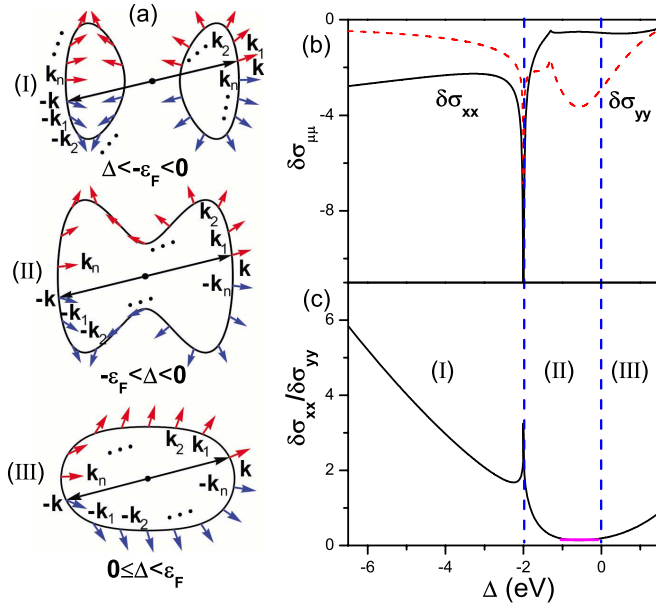


FIG. 4. (a) Schematic illustration of the backscattering processes along Fermi surface, where the red and blue arrows describe the spin rotation along the scattering path  $\mathbf{k} \rightarrow \mathbf{k}_1 \rightarrow \mathbf{k}_2 \rightarrow \dots \rightarrow -\mathbf{k}$ , and its time-reversal path  $-\mathbf{k} \rightarrow -\mathbf{k}_1 \rightarrow -\mathbf{k}_2 \rightarrow \dots \rightarrow \mathbf{k}$ , respectively. The corrections of quantum conductivities  $\delta\sigma_{\mu\mu}$  ( $\mu = x, y$ ) in (b) and their ratio  $\delta\sigma_{xx}/\delta\sigma_{yy}$  in (c) on the merging parameter  $\Delta$  are shown at  $k_B T = 0.3$  eV. The other parameters are the same as those in Fig. 3.

further reduced as

$$\tau_0/\tau_\varepsilon = \kappa T, \quad (13)$$

where  $\kappa = \frac{1}{2\varepsilon_F} [\Lambda_1 \ln(2\varepsilon_F \tau_0 \Lambda_2 / \Lambda_1) + \Lambda_0]$ .

(ii) For  $\Delta \ll -\varepsilon_F$ , i.e., the case (I) in Fig. 1,  $\beta \approx 0$ , so the term on  $\omega_m$  in the numerator of Eq. (8) vanishes. Consequently, to the lowest order, the Coulomb interaction reduces to

$$V(\mathbf{q}, \omega_m) = \frac{V_0(q)[|\omega_m| - (\tau_0 \Delta / m)q_x^2 + \tau_0 v_y^2 q_y^2]}{|\omega_m| - V_0(q)[(\tau_0 \Delta / m)q_x^2 - \tau_0 v_y^2 q_y^2]}. \quad (14)$$

Evidently, Eq. (14) contains the bare Coulomb interaction term  $V_0(q)$ , which is different from Eq. (10) that is independent of the bare coupling constant  $e^2/\varepsilon$ . Performing a similar calculation like Eq. (12), we finally get

$$\frac{\tau_0}{\tau_\varepsilon} = \frac{AT}{2\varepsilon_F} [\lambda_1 \ln(BT\tau_\varepsilon^2) + \lambda_2], \quad (15)$$

where  $A = \frac{\sqrt{mv_y^2(-\Delta)}}{2\sqrt{2\pi(-\Delta + mv_y^2)}}$ ,  $B = (\frac{e^2}{v_y \varepsilon})^2 \frac{\tau_0 \varepsilon_F^3}{2\Delta^2} (mv_y^2 - \Delta)$ ,  $\lambda_1 = \int_0^{2\pi} d\varphi (1 + v \cos \varphi)^{-1}$ , and  $\lambda_2 = \int_0^{2\pi} d\varphi (1 + v \cos \varphi)^{-1} \ln(1 + v \cos \varphi)$ . To the leading order in  $T$ ,  $\tau_\varepsilon$  is further expressed as

$$\frac{\tau_0}{\tau_\varepsilon} = \frac{AT}{2\varepsilon_F} \left[ \lambda_1 \ln\left(\frac{T_0}{T}\right) + \lambda_2 \right], \quad (16)$$

where  $T_0 = 4(\varepsilon_F \tau_0)^2 B / (\lambda_1 A)^2$ .

The inelastic scattering time  $\tau_\varepsilon$  is determined by the screened Coulomb interaction that is dominated by the integral over the Fermi surface. From Fig. 4(a), one may observe

that at  $\Delta \geq 0$ , the Fermi surface is an ellipselike curve (lower panel), and with decreasing  $\Delta$ , its middle part shrinks, and then, it disrupts to two unconnected rings. This topological change of the Fermi surface is called the Lifshitz transition [49]. For the connected Fermi surface cases [cases (II) and (III)],  $1/\tau_\varepsilon$  shows a linear dependence on the temperature. However, corresponding to the unconnected Fermi surfaces [upper panel of Fig. 4(a), i.e., case (I)], a logarithmic factor  $T \ln T_0/T$  appears in  $1/\tau_\varepsilon$  [see Eq. (16)].

## V. RELATIONSHIP BETWEEN THE CONDUCTIVITY CORRECTIONS IN X AND Y DIRECTIONS

With an evolution of the parameter  $\Delta$ , the backscattering processes are shown in Fig. 4(a). The scattering paths  $\mathbf{k} \rightarrow \mathbf{k}_1 \rightarrow \mathbf{k}_2 \rightarrow \dots \rightarrow -\mathbf{k}$ , and  $-\mathbf{k} \rightarrow -\mathbf{k}_1 \rightarrow -\mathbf{k}_2 \rightarrow \dots \rightarrow \mathbf{k}$  are paired by the time-reversal symmetry, and form a loop in the momentum space that encloses two Dirac cones. The spin rotation is accompanied along the scattering paths [see the arrows of Fig. 4(a)]. With increasing the parameter  $\Delta$ , the system passes through different states from regions of  $\Delta < -\varepsilon_F < 0$  (case (I)),  $-\varepsilon_F < \Delta < 0$  [case (II)] to  $0 \leq \Delta < \varepsilon_F$  [case (III)]. No matter in which region, the spin rotates firstly in the counter clockwise direction, then turns to the clockwise direction, and finally recover to the counter clockwise direction. The net spin rotation in the whole process is equal to zero. Thus, the interference in such paths is constructive, as reflected in Fig. 4(b), the conductivity corrections  $\delta\sigma_{\mu\mu}$  are always negative in the full parameter regions, marking a WL behavior. For a comparison, only subject to the influence of the  $\delta$ -function impurity potentials, the WL phenomenon cannot appear in the usual Dirac system, where the scattering path surrounds single Dirac cone, and the net spin rotation is  $2\pi$ , contributing a Berry phase  $\pi$  to the backscattering, and thus the interference is destructive, leading to weak antilocalization [8,12,14]. Moreover, the above-mentioned WL can also be understood from the symmetry of the Hamiltonian that possesses the antiunitary symmetry  $\mathcal{T} = C$  with  $C$  the complex conjugation, i.e.,  $\mathcal{T}H(\mathbf{k})\mathcal{T}^{-1} = H(-\mathbf{k})$ , and belongs to the orthogonal class [12,50], which is an indication of WL.

The relation between  $\delta\sigma_{xx}$  and  $\delta\sigma_{yy}$  is uncovered by the ratio  $\delta\sigma_{xx}/\delta\sigma_{yy}$ , which linearly or nonlinearly depends on  $\Delta$  [Fig. 4(c)], separated by a sharp peak at  $\Delta = -\varepsilon_F$ . This characteristic behavior reflects the influence of the Lifshitz transition. The quantitative relation for  $\delta\sigma_{xx}$  and  $\delta\sigma_{yy}$  can be gained by studying the limiting cases of  $\Delta$  as follows:

(a) By analyzing the case of  $|\Delta| < \varepsilon_F$  which corresponds to the connected Fermi surfaces [see the middle and lower panels of Fig. 4(a), i.e., the cases (II) and (III)], the ratio  $\delta\sigma_{xx}/\delta\sigma_{yy}$  shows a parabolic dependence on  $\Delta$

$$\frac{\delta\sigma_{xx}}{\delta\sigma_{yy}} \approx \frac{\varepsilon_F}{3} \left[ \frac{\sqrt{3}}{2} \left( \frac{\Delta}{\varepsilon_F} \right)^2 + \frac{5}{13} \left( \frac{\Delta}{\varepsilon_F} \right) + \frac{5}{21} \right], \quad (17)$$

where the first and second term in square brackets are small at  $|\Delta| \ll \varepsilon_F$ , so they can be neglected, leading to a plateau at  $\delta\sigma_{xx}/\delta\sigma_{yy} = 5\varepsilon_F/63$ .

(b) At  $\Delta \ll -\varepsilon_F$  [The unconnected Fermi surfaces, case (I), upper panel of Fig. 4(a)], the conductivity corrections are

given by

$$\begin{aligned}\delta\sigma_{xx} &= -\frac{e^2}{\pi h} \frac{v_x}{\sqrt{2}v_y} \ln\left(\frac{\tau_\varepsilon}{\tau_0}\right), \\ \delta\sigma_{yy} &= -\frac{e^2}{\pi h} \frac{\sqrt{2}v_y}{v_x} \ln\left(\frac{\tau_\varepsilon}{\tau_0}\right),\end{aligned}\quad (18)$$

where  $v_x = \sqrt{2|\Delta|/m}$ , and the factor  $\sqrt{2}$  is attributed to the intervalley scattering occurring along the  $x$  direction [24]. From Eq. (18), we get  $\delta\sigma_{xx}/\delta\sigma_{yy} = -\Delta/mv_y^2$ .

## VI. SUMMARY

We study the quantum interference correction to conductivity within a semi-Dirac model across the merging transition of the Dirac points. It is found that  $\delta\sigma_{xx}$  and  $\delta\sigma_{yy}$  exhibit the WL behaviors, and there exists a linear or parabolic dependence on the merging parameter  $\Delta$  in the ratio  $\delta\sigma_{xx}/\delta\sigma_{yy}$ . We also calculate the inelastic scattering time  $\tau_\varepsilon$ , and find that the temperature dependence of  $\tau_\varepsilon$  exhibits a crossover from  $1/\tau_\varepsilon \sim T$  to  $T \ln T_0/T$  with decreasing  $\Delta$ . These phenomena are related to the Lifshitz transition that is governed by the relative magnitude between the Fermi energy and the merging parameter  $\Delta$ . The Fermi energy can be tuned independently by gate voltage [18,41–43], and  $\Delta$  can be changed by the external methods [28,38]. Thus, it is possible to experimentally observe the above predicted phenomena in 2D lattices. This present work provides a different perspective to understand weak localization through Lifshitz transition.

## ACKNOWLEDGMENTS

The work is supported by the Scientific Research Fund of Hunan Provincial Education Department (Grant No.18K051), and the Construct Program of the Key Discipline of Hunan Province. G.S. and Z-G.Z. are supported in part by the National Key R&D Program of China (Grant No. 2018YFA0305800), the Strategic Priority Research Program of CAS (Grants No. XDB28000000 and No. XDB33000000), and the NSFC (Grants No. 11834014, No. 11674317, and No. 11974348). Z-G.Z. is also supported by the Fundamental Research Funds for the Central Universities. YLH is supported by National Key R&D Program of China (No. 2018YFC1902401).

## APPENDIX A: THE DETAILS OF OUR THEORETICAL MODEL

The Hamiltonian is given by

$$H = \left( \Delta + \frac{k_x^2}{2m} \right) \sigma_x + v_y k_y \sigma_y. \quad (A1)$$

The corresponding Schrödinger's equation is

$$H|u_{\mathbf{k}}\rangle = E_{\mathbf{k}}|u_{\mathbf{k}}\rangle, \quad (A2)$$

where the eigenvalue is

$$E_{\mathbf{k}}^\pm = \pm \sqrt{\left( \Delta + \frac{k_x^2}{2m} \right)^2 + (v_y k_y)^2}, \quad (A3)$$

and the eigenfunctions are

$$|u_{\mathbf{k}}^+\rangle = \frac{\sqrt{2}}{2} \begin{pmatrix} 1 \\ e^{i\phi} \end{pmatrix} e^{i\mathbf{k}\cdot\mathbf{r}}, \quad (A4)$$

$$|u_{\mathbf{k}}^-\rangle = \frac{\sqrt{2}}{2} \begin{pmatrix} 1 \\ -e^{i\phi} \end{pmatrix} e^{i\mathbf{k}\cdot\mathbf{r}}. \quad (A5)$$

The operators of the velocity are given by

$$v_x = \frac{1}{\hbar m} k_x \sigma_x, \quad \tilde{v}_y = \frac{v_y}{\hbar} \sigma_y. \quad (A6)$$

We consider the model of randomly located  $\delta$ -function scatters:  $V(\mathbf{r}) = \sum_i V_i \delta(\mathbf{r} - \mathbf{R}_i)$  with  $\mathbf{R}_i$  the position of impurities. In the eigenstate representation, the velocity and disorder operators have the following matrix form:

$$\begin{aligned}v_x &= \begin{pmatrix} v_{\mathbf{k}^{++}}^x & v_{\mathbf{k}^{+-}}^x \\ v_{\mathbf{k}^{-+}}^x & v_{\mathbf{k}^{--}}^x \end{pmatrix}, \quad \tilde{v}_y = \begin{pmatrix} v_{\mathbf{k}^{++}}^y & v_{\mathbf{k}^{+-}}^y \\ v_{\mathbf{k}^{-+}}^y & v_{\mathbf{k}^{--}}^y \end{pmatrix}, \\ V_{\mathbf{k}'\mathbf{k}} &= \begin{pmatrix} V_{\mathbf{k}'\mathbf{k}}^{++} & V_{\mathbf{k}'\mathbf{k}}^{+-} \\ V_{\mathbf{k}'\mathbf{k}}^{-+} & V_{\mathbf{k}'\mathbf{k}}^{--} \end{pmatrix},\end{aligned}\quad (A7)$$

where

$$v_{\mathbf{k}^{++}}^x = \frac{k_x}{\hbar m} \cos \phi, \quad v_{\mathbf{k}^{+-}}^x = -\frac{ik_x}{\hbar m} \sin \phi, \quad (A8)$$

$$v_{\mathbf{k}^{-+}}^x = \frac{ik_x}{\hbar m} \sin \phi, \quad v_{\mathbf{k}^{--}}^x = -\frac{k_x}{\hbar m} \cos \phi, \quad (A9)$$

$$v_{\mathbf{k}^{++}}^y = v_y \sin \phi, \quad v_{\mathbf{k}^{+-}}^y = iv_y \cos \phi, \quad (A10)$$

$$v_{\mathbf{k}^{-+}}^y = -iv_y \cos \phi, \quad v_{\mathbf{k}^{--}}^y = -v_y \sin \phi, \quad (A11)$$

$$V_{\mathbf{k}'\mathbf{k}}^{++} = \frac{1}{2} V_0(\mathbf{k}' - \mathbf{k}) [1 + e^{i(\phi - \phi')}], \quad (A12)$$

$$V_{\mathbf{k}'\mathbf{k}}^{+-} = \frac{1}{2} V_0(\mathbf{k}' - \mathbf{k}) [1 - e^{i(\phi - \phi')}], \quad (A13)$$

$$V_{\mathbf{k}'\mathbf{k}}^{-+} = \frac{1}{2} V_0(\mathbf{k}' - \mathbf{k}) [1 - e^{i(\phi - \phi')}], \quad (A14)$$

$$V_{\mathbf{k}'\mathbf{k}}^{--} = \frac{1}{2} V_0(\mathbf{k}' - \mathbf{k}) [1 + e^{i(\phi - \phi')}], \quad (A15)$$

with  $V_0(\mathbf{q}) = \sum_i V_i e^{-i\mathbf{q}\cdot\mathbf{R}_i}$ .

## APPENDIX B: GREEN'S FUNCTIONS

Within the Born approximation, the retarded ( $R$ ) and advanced ( $A$ ) Green's functions are given by

$$G_{\mathbf{k}}^{R/A} = \frac{1}{\varepsilon_F - E_{\mathbf{k}} \pm i\hbar/(2\tau)}. \quad (B1)$$

Here, the impurity scattering time is defined as

$$\begin{aligned}\frac{1}{\tau} &= \frac{2\pi}{\hbar} \sum_{\mathbf{k}_1} \langle V_{\mathbf{k}\mathbf{k}_1}^{++} V_{\mathbf{k}_1\mathbf{k}}^{++} \rangle \delta(\varepsilon_F - E_{\mathbf{k}_1}) \\ &= \tau_0^{-1} (1 + \gamma \cos \phi),\end{aligned}\quad (B2)$$

where  $\tau_0^{-1} = \frac{\pi}{\hbar} n_i V_0^2 g_0$ , and  $\gamma = \mathcal{I}_1/\mathcal{I}_0$  with  $n_i$  denoting the impurity concentration, the density of states  $g_0 =$

$\frac{1}{(2\pi)^2 v_y} (2m\varepsilon_F)^{\frac{1}{2}} \mathcal{I}_0$ . For  $\delta = \Delta/\varepsilon_F < -1$ ,

$$\mathcal{I}_0 = \frac{4}{\sqrt{1-\delta}} K[\sqrt{2/(1-\delta)}],$$

$$\mathcal{I}_1 = \frac{4}{\sqrt{1-\delta}} \{(1-\delta)E[\sqrt{2/(1-\delta)}] + \delta K[\sqrt{2/(1-\delta)}]\},$$

and for  $|\delta| < 1$

$$\mathcal{I}_0 = 2\sqrt{2}K[\sqrt{(1-\delta)/2}],$$

$$\mathcal{I}_1 = 2\sqrt{2}\{2E[\sqrt{(1-\delta)/2}] - K[\sqrt{(1-\delta)/2}]\},$$

where  $E(x)$  ( $K(x)$ ) is the elliptic integral of the first (second) kind.

### APPENDIX C: THE VERTEX CORRECTION

Since the  $x$  component of the velocity is an odd function of  $k_x$ , there does not exist the renormalization for  $v_x$ . For the velocity along the  $y$  direction, the ladder corrections are presented by Fig. 2(e), and the corresponding vertex equation is expressed as

$$\Upsilon_{\mathbf{k}}^y = v_{\mathbf{k}++}^y + \int \frac{d^2k'}{(2\pi)^2} G_{\mathbf{k}'}^R |V_{\mathbf{k}\mathbf{k}'}^{++}|^2 G_{\mathbf{k}'}^A \Upsilon_{\mathbf{k}'}^y. \quad (\text{C1})$$

By iteration, we can suppose  $\Upsilon_{\mathbf{k}}^y = \alpha_0 v_y \sin \theta \sin \phi$ , and obtain

$$\alpha_0 = \frac{\mathcal{I}_0}{\mathcal{I}_0 - \mathcal{J}_1 + \mathcal{K}_2}, \quad (\text{C2})$$

where

$$\mathcal{K}_2 = \frac{1}{\gamma} \mathcal{I}_1 - \frac{1}{\gamma^2} \mathcal{I}_0 + \frac{1}{\gamma^2} \mathcal{J}_1, \quad (\text{C3})$$

and

$$\mathcal{J}_1 = \begin{cases} \frac{4}{(1+\gamma)\sqrt{1-\delta}} \Pi\left(\frac{\pi}{2}, \frac{2\gamma}{1+\gamma}, \sqrt{\frac{2}{1-\delta}}\right), & \delta < -1, \\ \frac{2\sqrt{2}}{(1+\gamma)} \Pi\left[\frac{\pi}{2}, \frac{\gamma(1-\delta)}{1+\gamma}, \sqrt{\frac{1-\delta}{2}}\right], & |\delta| < 1, \end{cases} \quad (\text{C4})$$

where  $\Pi$  is an elliptic integral of the third kind.

### APPENDIX D: COOPERON

The full Cooperon can be derived by solving the Bethe-Salpeter equation represented graphically in Fig. 2(d)

$$\Gamma_{\mathbf{k}\mathbf{k}'}(\mathbf{q}) = \Gamma_{\mathbf{k}\mathbf{k}'}^0 + \int \frac{d^2k_1}{(2\pi)^2} \Gamma_{\mathbf{k}\mathbf{k}_1}^0 G_{\mathbf{k}_1}^R G_{\mathbf{q}-\mathbf{k}_1}^A \Gamma_{\mathbf{k}_1\mathbf{k}'}(\mathbf{q}), \quad (\text{D1})$$

where the bare Cooperon reads

$$\Gamma_{\mathbf{k}\mathbf{k}'}^0 = \frac{\hbar}{2\pi g_0 \tau_0} [1 + \cos(\phi - \phi')]. \quad (\text{D2})$$

By iteration, one can find that the full Cooperon can be written in the form of

$$\begin{aligned} \Gamma_{\mathbf{k}\mathbf{k}'}(\mathbf{q}) = & \frac{\hbar}{2\pi g_0 \tau_0} (\gamma_0 + \gamma_1 \cos \phi + \gamma_2 \sin \phi + \gamma_3 \cos \phi' \\ & + \gamma_4 \sin \phi' + \gamma_5 \cos \phi \cos \phi' + \gamma_6 \cos \phi \sin \phi' \\ & + \gamma_7 \sin \phi \cos \phi' + \gamma_8 \sin \phi \sin \phi'). \end{aligned} \quad (\text{D3})$$

After some straightforward but lengthy algebraic calculations, by keeping the most divergent terms in the limit of  $\mathbf{q} \rightarrow 0$ , we find

$$\Gamma_{\mathbf{k}\mathbf{k}'}(\mathbf{q}) = \frac{\hbar^3 \mathcal{I}_0}{2\pi g_0 \tau_0^3} \frac{1}{(2\varepsilon_F/m) D_x q_x^2 + v_y^2 D_y q_y^2}, \quad (\text{D4})$$

where

$$D_x = \mathcal{K}_8 + 2\gamma \mathcal{K}_9 - \frac{\gamma \mathcal{K}_1 (\mathcal{K}_8 - \mathcal{K}_{10})}{\mathcal{I}_0 - \mathcal{J}_1 + \mathcal{K}_2}, \quad (\text{D5})$$

and

$$D_y = \mathcal{K}_5 + 2\gamma \mathcal{K}_6 + \frac{\mathcal{K}_3^2}{\mathcal{I}_0 - \mathcal{J}_1 + \mathcal{K}_2} - \frac{\gamma (\mathcal{K}_1 \mathcal{K}_7 + 2\mathcal{K}_3 \mathcal{K}_4)}{\mathcal{I}_0 - \mathcal{J}_1 + \mathcal{K}_2}, \quad (\text{D6})$$

with

$$\mathcal{K}_1 = \frac{1}{\gamma} (\mathcal{I}_0 - \mathcal{J}_1), \quad (\text{D7})$$

$$\mathcal{K}_3 = -\frac{1}{\gamma^2} \mathcal{I}_0 + \frac{2}{\gamma^2} \mathcal{J}_1 + \left(1 - \frac{1}{\gamma^2}\right) \mathcal{J}_2, \quad (\text{D8})$$

$$\mathcal{K}_4 = \frac{2\mathcal{I}_0}{\gamma^3} - \frac{\mathcal{I}_1}{\gamma^2} + \left(\frac{1}{\gamma} - \frac{3}{\gamma^3}\right) \mathcal{J}_1 - \left(\frac{1}{\gamma} - \frac{1}{\gamma^3}\right) \mathcal{J}_2, \quad (\text{D9})$$

$$\mathcal{K}_5 = \left(1 - \frac{1}{\gamma^2}\right) \mathcal{J}_3 - \frac{\mathcal{J}_1}{\gamma^2} + \frac{2\mathcal{J}_2}{\gamma^2}, \quad (\text{D10})$$

$$\mathcal{K}_6 = \frac{1}{\gamma} \left[ \frac{3\mathcal{J}_1}{\gamma^2} - \frac{\mathcal{I}_0}{\gamma^2} + \left(1 - \frac{3}{\gamma^2}\right) \mathcal{J}_2 - \left(1 - \frac{1}{\gamma^2}\right) \mathcal{J}_3 \right], \quad (\text{D11})$$

$$\begin{aligned} \mathcal{K}_7 = & \left(\frac{6}{\gamma^4} - \frac{2}{\gamma^2}\right) \mathcal{J}_1 + \left(\frac{4}{\gamma^2} - \frac{4}{\gamma^4}\right) \mathcal{J}_2 \\ & + \left(1 - \frac{1}{\gamma^2}\right) \mathcal{J}_3 + \frac{1}{\gamma^3} \left(\mathcal{I}_1 - \frac{3\mathcal{I}_0}{\gamma}\right), \end{aligned} \quad (\text{D12})$$

$$\begin{aligned} \mathcal{K}_8 = & \frac{1}{\gamma^2} \left[ \frac{\mathcal{I}_0}{\gamma} - \left(\frac{3}{\gamma} + \frac{\Delta}{\varepsilon_F}\right) \mathcal{J}_1 + \left(\frac{3}{\gamma} + \frac{2\Delta}{\varepsilon_F}\right) \mathcal{J}_2 \right. \\ & \left. - \left(\frac{1}{\gamma} + \frac{\Delta}{\varepsilon_F}\right) \mathcal{J}_3 \right], \end{aligned} \quad (\text{D13})$$

$$\begin{aligned} \mathcal{K}_9 = & \frac{1}{\gamma^3} \left\{ \mathcal{I}_1 - \left(\frac{3}{\gamma} + \frac{\Delta}{\varepsilon_F}\right) \mathcal{I}_0 + \left(\frac{6}{\gamma} + \frac{3\Delta}{\varepsilon_F}\right) \mathcal{J}_1 \right. \\ & \left. - \left(\frac{4}{\gamma} + \frac{3\Delta}{\varepsilon_F}\right) \mathcal{J}_2 + \left(\frac{1}{\gamma} + \frac{\Delta}{\varepsilon_F}\right) \mathcal{J}_3 \right\}, \end{aligned} \quad (\text{D14})$$

$$\begin{aligned} \mathcal{K}_{10} = & \frac{1}{\gamma^3} \left[ \mathcal{I}_2 - \left(\frac{3}{\gamma} + \frac{\Delta}{\varepsilon_F}\right) \mathcal{I}_1 + \left(\frac{6}{\gamma^2} + \frac{3\Delta}{\varepsilon_F \gamma}\right) \mathcal{I}_0 \right. \\ & \left. - \left(\frac{10}{\gamma^2} + \frac{6\Delta}{\varepsilon_F \gamma}\right) \mathcal{J}_1 + \left(\frac{5}{\gamma^2} + \frac{4\Delta}{\varepsilon_F \gamma}\right) \mathcal{J}_2 \right. \\ & \left. - \left(\frac{1}{\gamma^2} + \frac{\Delta}{\varepsilon_F \gamma}\right) \mathcal{J}_3 \right], \end{aligned} \quad (\text{D15})$$

$$\begin{aligned} \mathcal{J}_2 = & -\frac{1}{2(1-\gamma^2)(1+\gamma\delta)} (\mathcal{I}_0 + \gamma \mathcal{I}_1) \\ & + \frac{3 + 2\gamma\delta - \gamma^2}{2(1-\gamma^2)(1+\gamma\delta)} \mathcal{J}_1, \end{aligned} \quad (\text{D16})$$

$$\begin{aligned} \mathcal{J}_3 = & \frac{1}{4(1-\gamma^2)(1+\gamma\delta)} \mathcal{I}_0 - \frac{3+\gamma\delta}{2(1-\gamma^2)(1+\gamma\delta)} \mathcal{J}_1 \\ & + \frac{9+6\gamma\delta-3\gamma^2}{4(1-\gamma^2)(1+\gamma\delta)} \mathcal{J}_2. \end{aligned} \quad (\text{D17})$$

In the above expressions, for  $\delta < -1$ ,

$$\begin{aligned} \mathcal{I}_2 = & \frac{4}{3\sqrt{1-\delta}} \left\{ (2\delta^2+1)K\left(\sqrt{\frac{2}{1-\delta}}\right) \right. \\ & \left. + 2\delta(1-\delta)E\left(\sqrt{\frac{2}{1-\delta}}\right) \right\}, \end{aligned} \quad (\text{D18})$$

for  $|\delta| < 1$ ,

$$\mathcal{I}_2 = \frac{2\sqrt{2}}{3} \left\{ (1-2\delta)K\left(\sqrt{\frac{1-\delta}{2}}\right) + 4\delta E\left(\sqrt{\frac{1-\delta}{2}}\right) \right\}. \quad (\text{D19})$$

### APPENDIX E: QUANTUM INTERFERENCE CORRECTION TO CONDUCTIVITY

Considering the contribution of the bare and dressed Hikami boxes in Fig. 2, we derive the quantum interference correction to conductivity in  $x$  and  $y$  directions

$$\delta\sigma_{xx} = \frac{e^2\hbar}{2\pi} \sum_{\mathbf{k}\mathbf{q}} v_{\mathbf{k}+\mathbf{q}}^x G_{\mathbf{k}}^R G_{\mathbf{q}-\mathbf{k}}^A G_{\mathbf{q}-\mathbf{k}}^R G_{\mathbf{k}}^A v_{\mathbf{q}-\mathbf{k}+\mathbf{q}}^x \Gamma_{\mathbf{k},\mathbf{q}-\mathbf{k}}(\mathbf{q}), \quad (\text{E1})$$

$$\delta\sigma_{yy} = \delta\sigma_{yy}^B + 2\delta\sigma_{yy}^D, \quad (\text{E2})$$

where

$$\delta\sigma_{yy}^B = \frac{e^2\hbar}{2\pi} \sum_{\mathbf{k}\mathbf{q}} \Upsilon_{\mathbf{k}}^y G_{\mathbf{k}}^R G_{\mathbf{q}-\mathbf{k}}^A G_{\mathbf{q}-\mathbf{k}}^R G_{\mathbf{k}}^A \Upsilon_{\mathbf{q}-\mathbf{k}}^y \Gamma_{\mathbf{k},\mathbf{q}-\mathbf{k}}(\mathbf{q}) \quad (\text{E3})$$

and

$$\begin{aligned} \delta\sigma_{yy}^D = & \frac{e^2\hbar}{2\pi} \sum_{\mathbf{k}_1\mathbf{k}_2\mathbf{q}} \Upsilon_{\mathbf{q}-\mathbf{k}_2}^y G_{\mathbf{q}-\mathbf{k}_2}^R G_{\mathbf{k}_1}^R \langle V_{\mathbf{q}-\mathbf{k}_2,\mathbf{k}_1}^{++} V_{\mathbf{k}_2,\mathbf{q}-\mathbf{k}_1}^{++} \rangle \\ & \times G_{\mathbf{k}_2}^R G_{\mathbf{q}-\mathbf{k}_1}^R \Upsilon_{\mathbf{q}-\mathbf{k}_1}^y G_{\mathbf{q}-\mathbf{k}_1}^A G_{\mathbf{q}-\mathbf{k}_2}^A \Gamma_{\mathbf{k}_1\mathbf{k}_2}(\mathbf{q}) \end{aligned} \quad (\text{E4})$$

come from the bare and dressed Hikami boxes, respectively. Since the summation over  $\mathbf{k}$  contains the odd function of  $k_x$ , the contribution from the dressed Hikami boxes vanishes for the conductivity correction in the  $x$  direction. Substituting Eq. (D4) in Eqs. (E1), (E3) and (E4), then carrying out the integral, we get

$$\delta\sigma_{xx} = -\frac{e^2}{\pi h} \sqrt{\frac{2\varepsilon_F}{mv_y^2}} \frac{\mathcal{K}_8}{\bar{D}} \ln\left(\frac{\tau_\varepsilon}{\tau_0}\right) \quad (\text{E5})$$

and

$$\delta\sigma_{yy} = -\frac{e^2}{\pi h} \sqrt{\frac{mv_y^2}{2\varepsilon_F}} \frac{\alpha_0^2}{\bar{D}} \left( \mathcal{K}_5 - \frac{\mathcal{K}_3^2}{I_0} \right) \ln\left(\frac{\tau_\varepsilon}{\tau_0}\right), \quad (\text{E6})$$

where  $\bar{D} = \sqrt{D_x D_y}$ , and  $\tau_\varepsilon$  is the inelastic scattering time.

### APPENDIX F: INELASTIC SCATTERING TIME

The inelastic scattering time is related to the electron-electron interaction. Firstly, we introduce the Coulomb

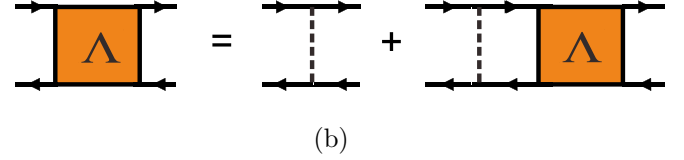
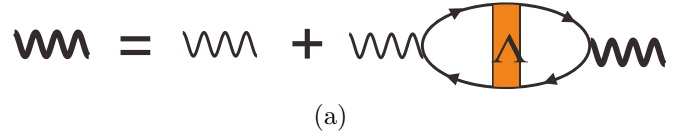


FIG. 5. The Feynman diagrams for the electron-electron interaction (a) and the particle-hole diffusion propagators (b).

interaction, which in the eigenstate representation is given by

$$\begin{aligned} V = & \frac{1}{2} \sum_{\mathbf{k}_1\mathbf{k}_2\mathbf{q}} V(\mathbf{q}) \langle u_{\mathbf{k}_2-\mathbf{q}}^+ | u_{\mathbf{k}_2}^+ \rangle \langle u_{\mathbf{k}_1+\mathbf{q}}^+ | u_{\mathbf{k}_1}^+ \rangle a_{\mathbf{k}_1+\mathbf{q}}^\dagger a_{\mathbf{k}_2-\mathbf{q}}^\dagger a_{\mathbf{k}_2} a_{\mathbf{k}_1} \\ \approx & \frac{1}{2} \sum_{\mathbf{k}_1\mathbf{k}_2\mathbf{q}} V(\mathbf{q}) a_{\mathbf{k}_1+\mathbf{q}}^\dagger a_{\mathbf{k}_2-\mathbf{q}}^\dagger a_{\mathbf{k}_2} a_{\mathbf{k}_1}, \end{aligned} \quad (\text{F1})$$

where  $V(\mathbf{q}) = \frac{e^2}{2\varepsilon q}$ . In the presence of the impurity scattering, the dressed interaction corresponding to the Feynman diagram of Fig. 5(a) is expressed as

$$V(\mathbf{q}, \omega_m) = \frac{V_0(\mathbf{q})}{1 + V_0(\mathbf{q})\Pi(\mathbf{q}, \omega_m)}, \quad (\text{F2})$$

where the orange region presents the particle-hole diffusion,

$$\begin{aligned} \Lambda_{\mathbf{k}\mathbf{k}'}(\mathbf{q}) = & \Lambda_{\mathbf{k}\mathbf{k}'}^0 + \frac{1}{S} \sum_{\mathbf{k}_1} \Lambda_{\mathbf{k}\mathbf{k}_1}^0 G_{\mathbf{k}_1+\mathbf{q}}(i\varepsilon_n + i\omega_m) G_{\mathbf{k}_1}(i\varepsilon_n) \Lambda_{\mathbf{k}_1\mathbf{k}'}(\mathbf{q}). \end{aligned} \quad (\text{F3})$$

Similar to the calculation of Eq. (D1), in the limit of  $\mathbf{q} \rightarrow 0$  and  $\omega_m \rightarrow 0$ , we acquire

$$\Lambda_{\mathbf{k},\mathbf{k}'}(\mathbf{q}) = \frac{\hbar^2 I_0}{2\pi g_0 \tau_0^2} \frac{1}{I_0 |\omega_m| + \frac{2\varepsilon_F \tau_0}{m} D_x q_x^2 + v_y^2 \tau_0 D_y q_y^2}. \quad (\text{F4})$$

The density-density response function is dressed via the particle-hole diffusion and takes the form of

$$\Pi(\mathbf{q}, \omega_m) = \frac{g_0 [\beta |\omega_m| + (2\tau_0 \varepsilon_F / m) D_x q_x^2 + \tau_0 v_y^2 D_y q_y^2]}{I_0 |\omega_m| + (2\tau_0 \varepsilon_F / m) D_x q_x^2 + \tau_0 v_y^2 D_y q_y^2}. \quad (\text{F5})$$

Considering all the contributions from Fig. 6, we find

$$\begin{aligned} \frac{1}{\tau_\varepsilon} = & \frac{T}{2\pi g_0 \tau_0^2} \left[ 2 \left( \frac{2\pi g_0}{I_0} \right)^3 \mathcal{J}_1^2 \mathcal{J}_3 \right. \\ & - \frac{\mathcal{J}_2^2 + \mathcal{K}_{11}^2}{I_0} \tau_0^5 \sum_{m,\mathbf{q}} \Lambda^2(\mathbf{q}) V(\mathbf{q}, \omega_m) \\ & \left. - \left( 2\pi \frac{g_0}{I_0} \mathcal{J}_2 \tau_0^2 \right)^2 \sum_{m,\mathbf{q}} \Gamma(\mathbf{q}) V(\mathbf{q}, \omega_m) \right], \end{aligned} \quad (\text{F6})$$

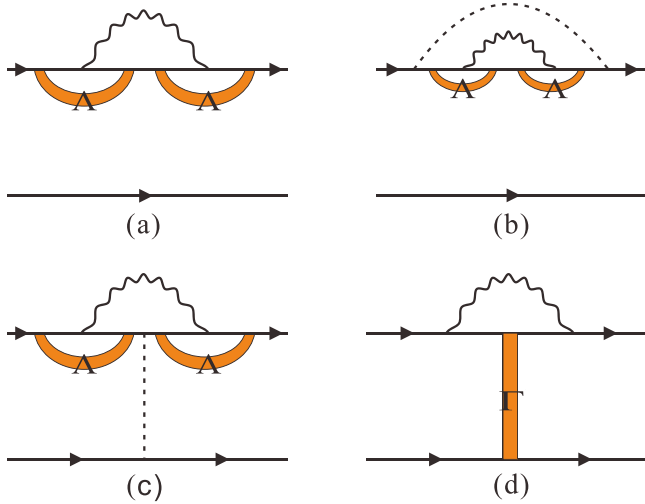


FIG. 6. The Feynman diagrams for the scattering processes contributing to the inelastic scattering time due to electron-electron interaction, where orange arc and rectangle represent particle-hole and particle-particle propagators, respectively.

where  $\mathcal{K}_{11} = (\mathcal{J}_1 - \mathcal{J}_2)/\gamma$ , and we use the abbreviated symbols  $\Lambda(\mathbf{q})$  and  $\Gamma(\mathbf{q})$  for  $\Lambda_{\mathbf{k},\mathbf{k}'}(\mathbf{q})$  and  $\Gamma_{\mathbf{k},\mathbf{k}'}(\mathbf{q})$ . By performing the analytic continuations and substituting  $\Lambda(\mathbf{q})$  and  $\Gamma(\mathbf{q})$ , Eq. (F6) becomes

$$\begin{aligned} \frac{1}{\tau_\varepsilon} = & -\frac{\mathcal{J}_1^2 T}{8\pi^3 g_0 V_+} \text{Im} \int_0^{2\pi} d\varphi \frac{1}{1 + \nu \cos \varphi} \\ & \times \int_0^\infty dy \sum_{s=\pm} \left[ \frac{1}{\mathcal{I}_0 y + s(\alpha y^{1/2} + \beta)(\frac{\tau_0}{\tau_\varepsilon} + y)} \right. \\ & \left. \times \log \frac{\mathcal{I}_0 T \tau_0 + i(\frac{\tau_0}{\tau_\varepsilon} + y)}{-s(\alpha y^{1/2} + \beta) T \tau_0 + iy} \right], \end{aligned} \quad (\text{F7})$$

where  $V_+ = \frac{1}{2} \tau_0 v_y^2 [(2\varepsilon_F/mv_y^2)D_x + D_y]$ , and  $\alpha = \frac{\mathcal{I}_0}{\sqrt{\mathcal{A}(1+\nu \cos \varphi)}}$  with  $\mathcal{A} = (\frac{e^2 g_0}{2\varepsilon})^2 V_+ \tau_0$  and  $\nu = \frac{D_x - (mv_y^2/2\varepsilon_F)D_y}{D_x + (mv_y^2/2\varepsilon_F)D_y}$ .

For  $|\Delta| < \varepsilon_F$ , keeping the leading terms on small  $\omega_m$  and  $q$ , we obtain

$$V(\mathbf{q}, \omega_m) = \frac{\mathcal{I}_0 |\omega_m| + (2\tau_0 \varepsilon_F/m) D_x q_x^2 + \tau_0 v_y^2 D_y q_y^2}{g_0 \beta |\omega_m| + (2\tau_0 \varepsilon_F/m) D_x q_x^2 + \tau_0 v_y^2 D_y q_y^2}. \quad (\text{F8})$$

Substituting Eq. (F8) into Eq. (F6), we have

$$\begin{aligned} \frac{\tau_0}{\tau_\varepsilon} = & \frac{\chi}{\varepsilon_F} \int_0^T dz \frac{z}{\sinh z/T} \left[ \frac{-i\mathcal{I}_0 z + \frac{1}{\tau_\varepsilon}}{\beta^2 z^2 + (-i\mathcal{I}_0 z + \frac{1}{\tau_\varepsilon})^2} \right. \\ & \left. \times \ln \frac{-i\mathcal{I}_0 z + \frac{1}{\tau_\varepsilon}}{\beta z} + \frac{\pi \beta z/2}{\beta^2 z^2 + (-i\mathcal{I}_0 z + \frac{1}{\tau_\varepsilon})^2} \right]. \end{aligned} \quad (\text{F9})$$

Replacing  $(\sinh z/T)^{-1}$  with  $T/z$  at  $\tau_\varepsilon T \gg 1$ , the estimation for Eq. (F9) gives

$$\frac{\tau_0}{\tau_\varepsilon} = \frac{T}{2\varepsilon_F} [\Lambda_1 \ln(\Lambda_2 T \tau_\varepsilon) + \Lambda_0], \quad (\text{F10})$$

where  $\Lambda_1 = \frac{\pi \mathcal{J}_1^2}{(2\mathcal{I}_0^2 - \mathcal{J}_1^2) \mathcal{D}}$ ,  $\Lambda_2 = (2\mathcal{I}_0^2 - \mathcal{J}_1^2)/\mathcal{I}_0$ , and  $\Lambda_0 = \frac{\pi \mathcal{I}_0^2}{(2\mathcal{I}_0^2 - \mathcal{J}_1^2) \mathcal{D}} \ln(\frac{\mathcal{I}_0^2}{\mathcal{I}_0^2 - \mathcal{J}_1^2})$ . Whence, to leading order in  $T$ , we obtain

$$\frac{\tau_0}{\tau_\varepsilon} = \kappa T, \quad (\text{F11})$$

where  $\kappa = \frac{1}{2\varepsilon_F} [\Lambda_1 \ln(2\varepsilon_F \tau_0 \Lambda_2/\Lambda_1) + \Lambda_0]$ . The same calculation process as the above is used for the case of  $\Delta \ll -\varepsilon_F$ , resulting in

$$\frac{\tau_0}{\tau_\varepsilon} = \frac{AT}{2\varepsilon_F} [\lambda_1 \ln(BT \tau_\varepsilon^2) + \lambda_2], \quad (\text{F12})$$

where  $A = \frac{\sqrt{mv_y^2(-\Delta)}}{2\sqrt{2\pi(-\Delta + mv_y^2)}}$ ,  $B = (\frac{e^2}{v_y \varepsilon})^2 \frac{\tau_0 \varepsilon_F^3}{2\Delta^2} (mv_y^2 - \Delta)$ ,  $\lambda_1 = \int_0^{2\pi} d\varphi (1 + \nu \varphi)^{-1}$ , and  $\lambda_2 = \int_0^{2\pi} d\varphi (1 + \nu \cos \varphi)^{-1} \ln(1 + \nu \cos \varphi)$ . Then to the leading order in  $T$ , we get

$$\frac{\tau_0}{\tau_\varepsilon} = \frac{AT}{2\varepsilon_F} \left[ \lambda_1 \ln\left(\frac{T_0}{T}\right) + \lambda_2 \right], \quad (\text{F13})$$

where  $T_0 = 4(\varepsilon_F \tau_0)^2 B/(\lambda_1 A)^2$ .

[1] For a review, see G. Bergmann, *Phys. Rep.* **107**, 1 (1983).  
[2] K. S. Novoselov, A. K. Geim, S. V. Morozov, D. Jiang, M. I. Katsnelson, I. V. Grigorieva, S. V. Dubonos, and A. A. Firsov, *Nature (London)* **438**, 197 (2005).  
[3] Y. Zhang, Y.-W. Tan, H. L. Stormer, and P. Kim, *Nature (London)* **438**, 201 (2005).  
[4] Y. Zheng and T. Ando, *Phys. Rev. B* **65**, 245420 (2002).  
[5] V. P. Gusynin and S. G. Sharapov, *Phys. Rev. Lett.* **95**, 146801 (2005).  
[6] N. M. R. Peres, F. Guinea, and A. H. Castro Neto, *Phys. Rev. B* **73**, 125411 (2006).  
[7] For a review, see A. H. Castro Neto, F. Guinea, N. M. R. Peres, K. S. Novoselov, and A. K. Geim, *Rev. Mod. Phys.* **81**, 109 (2009).

[8] H. Suzuura and T. Ando, *Phys. Rev. Lett.* **89**, 266603 (2002).  
[9] A. K. Geim and K. S. Novoselov, *Nature Mater.* **6**, 183 (2007).  
[10] J. McClure, *Phys. Rev.* **104**, 666 (1956).  
[11] D. P. DiVincenzo and E. J. Mele, *Phys. Rev. B* **29**, 1685 (1984).  
[12] T. Ando, T. Nakanishi, and R. Saito, *J. Phys. Soc. Jap.* **67**, 2857 (1998).  
[13] A. H. Castro Neto, F. Guinea, and N. M. R. Peres, *Phys. Rev. B* **73**, 205408 (2006).  
[14] H. Z. Lu, W. Yao, D. Xiao, and S. Q. Shen, *Phys. Rev. Lett.* **110**, 016806 (2013).  
[15] K. Kechedzhi, E. McCann, V. I. Fal'ko, H. Suzuura, T. Ando, and B. L. Altshuler, *Eur. Phys. J. Special Topics* **148**, 39 (2007).  
[16] E. McCann, K. Kechedzhi, V. I. Fal'ko, H. Suzuura, T. Ando, and B. L. Altshuler, *Phys. Rev. Lett.* **97**, 146805 (2006).

- [17] V. I. Fal'ko, K. Kechedzhi, E. McCann, B. L. Altshuler, H. Suzuura, and T. Ando, *Solid State Commun.* **143**, 33 (2007).
- [18] S. V. Morozov, K. S. Novoselov, M. I. Katsnelson, F. Schedin, L. A. Ponomarenko, D. Jiang, and A. K. Geim, *Phys. Rev. Lett.* **97**, 016801 (2006).
- [19] A. F. Morpurgo and F. Guinea, *Phys. Rev. Lett.* **97**, 196804 (2006).
- [20] G. Montambaux, F. Piéchon, J. N. Fuchs, and M. O. Goerbig, *Phys. Rev. B* **80**, 153412 (2009); *Eur. Phys. J. B* **72**, 509 (2009).
- [21] R. D. Gail, J. N. Fuchs, M. O. Goerbig, F. Piéchon, and G. Montambaux, *Phys. B: Condens. Matter* **407**, 1948 (2012).
- [22] B. Wunsch, F. Guinea, and F. Sols, *New J. Phys.* **10**, 103027 (2008).
- [23] Y. Hasegawa, R. Konno, H. Nakano, and M. Kohmoto, *Phys. Rev. B* **74**, 033413 (2006).
- [24] P. Adroguer, D. Carpentier, G. Montambaux, and E. Orignac, *Phys. Rev. B* **93**, 125113 (2016).
- [25] P. Dietl, F. Piéchon, and G. Montambaux, *Phys. Rev. Lett.* **100**, 236405 (2008).
- [26] L. K. Lim, J. N. Fuchs, and G. Montambaux, *Phys. Rev. Lett.* **108**, 175303 (2012).
- [27] K. H. Ding, L. K. Lim, G. Su, and Z. Y. Weng, *Phys. Rev. B* **97**, 035123 (2018).
- [28] L. Tarruell, D. Greif, T. Uehlinger, G. Jotzu, and T. Esslinger, *Nature (London)* **483**, 302 (2012).
- [29] M. C. Rechtsman, Y. Plotnik, J. M. Zeuner, D. Song, Z. Chen, A. Szameit, and M. Segev, *Phys. Rev. Lett.* **111**, 103901 (2013).
- [30] M. Bellec, U. Kuhl, G. Montambaux, and F. Mortessagne, *Phys. Rev. Lett.* **110**, 033902 (2013).
- [31] S. Katayama, A. Kobayashi, and Y. Suzumura, *J. Phys. Soc. Jpn.* **75**, 054705 (2006).
- [32] A. Kobayashi, Y. Suzumura, F. Piéchon, and G. Montambaux, *Phys. Rev. B* **84**, 075450 (2011).
- [33] Y. Suzumura, T. Morinari, and F. Piéchon, *J. Phys. Soc. Jpn.* **82**, 023708 (2013).
- [34] V. Pardo and W. E. Pickett, *Phys. Rev. Lett.* **102**, 166803 (2009); *Phys. Rev. B* **81**, 035111 (2010).
- [35] S. Tang and M. S. Dresselhaus, *Nanoscale* **4**, 7786 (2012).
- [36] C. Kamal and M. Ezawa, *Phys. Rev. B* **91**, 085423 (2015).
- [37] R. Fei, V. Tran, and L. Yang, *Phys. Rev. B* **91**, 195319 (2015).
- [38] J. Kim, S. S. Baik, S. H. Ryu, Y. Sohn, S. Park, B.-G. Park, J. Denlinger, Y. Yi, H. J. Choi, and K. S. Kim, *Science* **349**, 723 (2015).
- [39] K. K. Gomes, W. Mar, W. Ko, F. Guinea, and H. C. Manoharan, *Nature (London)* **483**, 306 (2012).
- [40] M. Polini, F. Guinea, M. Lewenstein, H. C. Manoharan, and V. Pellegrini, *Nature Nanotech.* **8**, 625 (2013).
- [41] H. Z. Lu, J. Shi, and S. Q. Shen, *Phys. Rev. Lett.* **107**, 076801 (2011).
- [42] J. Chen, H. J. Qin, F. Yang, J. Liu, T. Guan, F. M. Qu, G. H. Zhang, J. R. Shi, X. C. Xie, C. L. Yang, K. H. Wu, and Y. Q. Li, and L. Lu, *Phys. Rev. Lett.* **105**, 176602 (2010).
- [43] J. G. Checkelsky, Y. S. Hor, R. J. Cava, and N. P. Ong, *Phys. Rev. Lett.* **106**, 196801 (2011).
- [44] S. Hikami, A. I. Larkin, and Y. Nagaoka, *Prog. Theor. Phys.* **63**, 707 (1980).
- [45] B. L. Altshuler, D. Khmelnitzkii, A. I. Larkin, and P. A. Lee, *Phys. Rev. B* **22**, 5142 (1980).
- [46] H. Bruus and K. Flensburg, *Many-Body Quantum Theory in Condensed Matter Physics: An Introduction* (Oxford University Press, Oxford, 2004).
- [47] Z. Z. Du, C. M. Wang, S. Li, H. Z. Lu, and X. C. Xie, *Nat. Commun.* **10**, 3047 (2019); C. Xiao, Z. Z. Du, and Q. Niu, *Phys. Rev. B* **100**, 165422 (2019).
- [48] E. Abrahams, P. W. Anderson, P. A. Lee, and T. V. Ramakrishnan, *Phys. Rev. B* **24**, 6783 (1981); H. Fukuyama and E. Abrahams, *ibid.* **27**, 5976 (1983); J. M. B. Lopes dos Santos, *ibid.* **28**, 1189 (1983).
- [49] I. M. Lifshitz, *Sov. Phys. JETP* **11**, 1130 (1960).
- [50] M. R. Zirnbauer, *J. Math. Phys.* **37**, 4986 (1996).